Breaking phase focused wave group loads on offshore wind turbine monopiles

Ghadirian, Amin; Bredmose, Henrik; Dixen, M.

Published in:
Journal of Physics: Conference Series (Online)

Link to article, DOI:
10.1088/1742-6596/753/9/092004

Publication date:
2016

Document Version
Publisher's PDF, also known as Version of record

Breaking phase focused wave group loads on offshore wind turbine monopiles

2016 J. Phys.: Conf. Ser. 753 092004

(http://iopscience.iop.org/1742-6596/753/9/092004)

Breaking phase focused wave group loads on offshore wind turbine monopiles

A. Ghadirian[1], H. Bredmose[1], M. Dixen[2]

[1] DTU Wind Energy, Nils Koppels Alle Building 403, DK-2800 Kgs. Lyngby, Denmark
[2] DHI, Agern Alle 5, DK-2970 Hørsholm, Denmark

E-mail: amgh@dtu.dk

Abstract. The current method for calculating extreme wave loads on offshore wind turbine structures is based on engineering models for non-breaking regular waves. The present article has the aim of validating previously developed models at DTU, namely the OceanWave3D potential flow wave model and a coupled OceanWave3D-OpenFOAM solver, against measurements of focused wave group impacts on a monopile. The focused 2D and 3D wave groups are reproduced and the free surface elevation and the in-line forces are compared to the experimental results. In addition, the pressure distribution on the monopile is examined at the time of maximum force and discussed in terms of shape and magnitude. Relative pressure time series are also compared between the simulations and experiments and detailed pressure fields for a 2D and 3D impact are discussed in terms of impact type. In general a good match for free surface elevation, in-line force and wave-induced pressures is found.

1. Introduction

Cost-reduction for the substructures is an important part in reducing the cost of offshore wind energy. A central element here is an accurate determination of the Ultimate Limit State wave loads with limited uncertainty. The current method for calculating such loads is to use the stream function theory [1] combined with a background sea state time series. This method is easy to implement and benefits from limited complexity in the parameters that should be chosen. However, the stream function theory is associated with assumptions such as 2D wave motion, symmetry in the crest of the waves, periodicity and a flat sea bed. This approach also neglects the effect of breaking waves which is the focus of this study. To overcome these, other nonlinear models are developed. However these models are not still vastly used in the industry, partly because of only limited validation against design cases.

Christensen et. al. [2] investigated the wave forces and wave run-up from large regular waves on an offshore wind-turbine foundation on a sloping bed by application of an in-house developed Navier-Stokes solver. They used the Volume Of Fluid method (VOF) to capture the free surface. The free surface elevation and run-ups reproduced by the model showed a good agreement with experimental reference results. A good agreement was also found between the small wave height maximum force with linear diffraction theory and the Morison equation [3].

Bredmose et. al. [4] investigated the impact of irregular waves on a current on a gravity wind turbine foundation. The results were compared to experiments. Furthermore, Bredmose and Jacobsen [5] used the InterFOAM solver of OpenFOAM to perform a numerical investigation of breaking wave impacts on an offshore wind turbine foundation in intermediate water depth. In

this study they used the focused wave group technique to reproduce the most probable extreme wave in the given sea state. The resulting in-line forces were compared to results from the linear theory and the Morison equation. It was seen that the in-line forces estimate by the latter method gave smaller peaks than the CFD results. They also extended the study [6] by investigating the vertical wave impacts on offshore wind turbine inspection platforms. However, both studies lacked the validation of the numerical results against experiments.

Hildebrandt and Schlurmann [7] used Ansys CFX model to reproduce wave breaking local pressures and forces on a tripod support structure. The study investigated the interaction of different types of breaking waves with the structure. A good agreement was shown for most of the cases between the impact pressure distributions seen in the experiments and in the numerical simulations.

The main goal of the present article, as part of the DeRisk project [8], is to provide systematic validations for two other open source models specially in case of breaking waves. One validated model is the fully nonlinear potential flow solver OceanWave3D [9] which is able to create 3D nonlinear waves in a relatively big domain. This model has also been coupled to the OpenFOAM tool box, Waves2FOAM [10] , by Paulsen et al. [11, 12]. This coupled solver is investigated in this study as the second model. Validation cases for regular waves and the Waves2FOAM toolbox have already been presented by [13] which also studied the mechanism for creation of the secondary load cycle, that creates an additional force peak after the main wave impact. The paper of Paulsen et al [11] presents validation cases of the coupled solver for four cases of regular, irregular and 2D phase focused waves and 2D focused wave group tests of Zang et. al. [14].

In the present paper, we provide further validation of the OceanWave3D and the coupled solver against new systematic measurements of focused wave group impacts on a monopile. Time series of free surface elevation and depth integrated forces are compared for two 2-dimensional and two 3-dimensional groups. Also the pressure distribution over the cylinder at the moment of impact by the focused wave is discussed. Computational pressure time series are further compared to measurements. Finally, the detailed pressure fields of a 2D and a 3D impact are discussed and linked to the type of impact.

2. Methodology

2.1. The experiments

The experiments were conducted in the shallow water basin at DHI Denmark at a scale ratio of 1:50. The full scale diameter of the monopile was 7 m and the full-scale depth of water was 33 m. The monopile was mounted on two force transducers — one at the top and one at the bottom — to measure the in-line force and the moment. Pressure sensors were installed facing the incident wave direction. In addition 31 wave gauges were installed to measure free surface elevation for the wave propagation towards the cylinder and around it. The monopile was placed 7.3 m from the wave makers (lab scale) and phase focused wave groups were created with their nominal linear focus point at the monopile center so that breaking and ringing forces could be measured. The wave generator was a piston wave maker driven with linear wave generation theory.

2.2. The numerical model

The coupled OceanWave3D and OpenFOAM solver [12] was used to reproduce the phase focused waves. Waves2Foam is a package added to OpenFOAMs InterFoam solver to allow generation of surface waves in relaxation zones close to the boundaries [10]. InterFoam uses a volume of fluid (VOF) method to treat the free surface flows [15].

To reproduce the experimental results the wave paddle velocity signal of the lab was used to produce the waves nonlinearly by the OceanWave3D solver. The signals were used as a flux boundary condition in the OceanWave3D domain. While this method of generation is linearly

consistent with the piston generation in the lab, differences at the second and higher orders can be expected due to the lack of piston movement in the numerical model. Good results with this approach, however, have been obtained in earlier works [5, 6, 13] and also in the context of the present campaign [8]. In figure 1, top views of the computational domains are shown for the 3D and 2D phase focused wave groups cases. For the 2D wave groups cases, the symmetry of the solution was utilized to reduce the OpenFOAM domain to half size. Even though the 3D focused wave group cases are also symmetric, a full domain was applied. In both cases, the embedded OpenFOAM domain was next driven with waves from OceanWave3D through a relaxation zone [10].

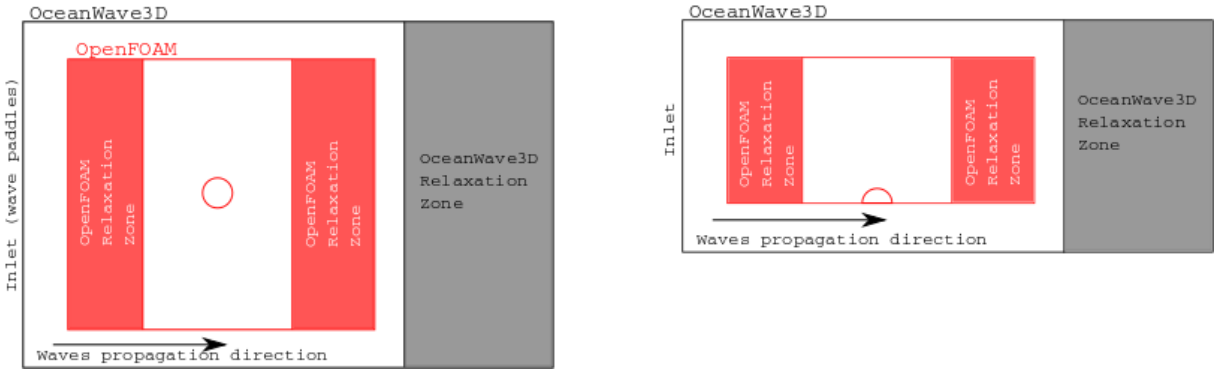

Figure 1: The computational domain for 3D (left) and 2D (right) phase focused wave groups.

3. Results

In table 1 the characteristics of the investigated wave groups are summarized. For all cases, a JONSWAP wave spectrum was used. The characteristic wave number, k_p, of each case was calculated using the given peak wave period, T_p, and the linear dispersion relation. The theoretical maximum wave height, H_{max}, was calculated using the relation $H_{max} = 1.86H_s$ [16] where H_s is the significant wave height. The spreading angle is defined as the maximum angle at which the wave components moved toward the nominal focus point in 3D for the focused wave groups. Obviously the spreading angle is zero for the 2D phase focused wave groups.

Table 1: Characteristics of the waves

	Full scale				Lab scale				
Case	h [m]	Hs [m]	Tp [s]	Spread angle [deg]	Ursell	k_pH_{max}	k_ph	$\frac{h}{gT_P^2}$	$\frac{H_{max}}{gT_P^2}$
204	33	7.5	12	13	13.3	0.49	1.1	0.023	0.0102
206	33	9.5	12	13	16.9	0.63	1.1	0.023	0.0129
209	33	7.5	12	0	13.3	0.49	1.1	0.023	0.0102
211	33	9.5	12	0	16.9	0.63	1.1	0.023	0.0129

The Ursell number, $Ur = \frac{HL^2}{h^3}$, in table 1 represents the nonlinearity of the waves while the k_pH_{max} measures the steepness of the waves. The cases 206 and 211 thus contained the most nonlinear and the steepest waves. The last two columns provide input to an assessment of the investigated waves in relation to a breaking criteria. This breaking criteria is calculated using

the following equation [17].

$$\frac{H_b}{gT_p^2} = A\{1 - \exp(-1.5\pi\frac{h}{L_p})\}\frac{\tanh(kh)}{2\pi} \quad (1)$$

Here H_b is the breaking wave height, T_p and L_p are the peak wave period and the peak wave length assuming a linear dispersion and constant water depth. Wave breaking for irregular waves occurs for $0.12 < A < 0.18$.

The wave conditions of the four tests are plotted together with the breaking criterion equation (1) in figure 2. Looking at this plot it can be seen that the cases 204 and 209 included less probable waves to break in 33 m deep water compared to cases 206 and 211. However all of the wave groups are predicted to contain breaking at some point.

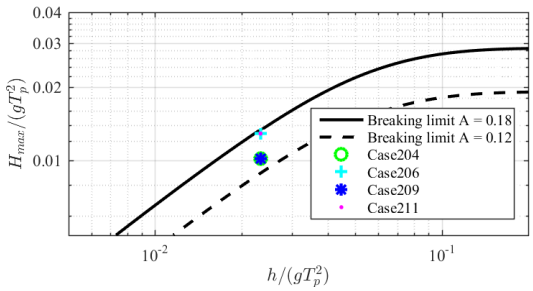

Figure 2: Characteristics of the investigated phase focused wave groups in relation to breaking criteria.

3.1. Free surface elevation

In figure 3 non-dimensional time series of the free surface elevation for all the investigated wave groups are presented. The cases on the left hand side, namely cases 209 and 211, are 2D focused wave groups while the ones on the right hand side, cases 204 and 206, are the 3D phase focused wave groups. It should be mentioned that the wave gauges in these cases are located 0.2 m upstream from the cylinder in both the physical and computational domains.

Looking at the blue curves in this figure, the wave gauges in the basin show the passage of the focused wave groups clearly by the increase in the oscillation amplitude of free surface elevation until the focus time. After the focus time the amplitude of surface elevation decreases again to reach $\eta = 0$. The time axis of all the plots have been shifted such that the focus time occurs at $\frac{t}{Tp} = 0$. It is clear that the focus wave height is larger in the cases 206 and 211, consistent with the larger significant wave height for these cases.

For the waves in figure 3 it can be seen that after the passage of the largest waves, a small crest occur within the next trough. After investigating the celerity of these bumps, using time series from neighboring wave gauges, and assuming a linear dispersion relation, it was found that the period of these small waves are about one third of the main incident waves. It was thus concluded that the nature of these small waves is the third-harmonic reflections of the main waves from the cylinder.

It is also worth mentioning that from the plots, the growth of surface elevation to the focus wave is more gradual in the 2D cases. This can be explained by knowing the process of phase focusing, in which a focused wave is created by superposition of many waves. In 3D cases these waves can come from different directions and simply join at the focus point, while for the 2D cases, all wave components come from the same direction and therefore have to focus through differences in phase speed.

From figure 3 it is clearly seen that in all of the cases the free surface elevation calculated by OceanWave3D is consistent with the ones from measurements in relation to phases and amplitude. Only minor differences can be seen between the OceanWave3D generated curves and the measurements.

However, it is seen that after the main wave groups pass the focus point, the surface elevation calms down in the measurements but the surface elevation in the OceanWave3D keeps oscillating for a longer time. A likely reason for this is reflection of waves from the lateral boundaries of the OceanWave3D model which were modelled as slip-walls.

Comparing the measurements and the OpenFOAM simulations in the same figure it is seen that the phases and the amplitudes of the OpenFOAM surface elevations are generally consistent with the measurements. However it can be seen that the surface elevation was marginally over-predicted in the troughs of the waves by OpenFOAM in all cases.

It is worth mentioning that the third order harmonic reflected waves can also be seen in the OpenFOAM simulations with the same order of magnitude and phase as in the measurements. In the OceanWave3D computations, however, these waves cannot be seen as no monopile was present in the domain of OceanWave3D.

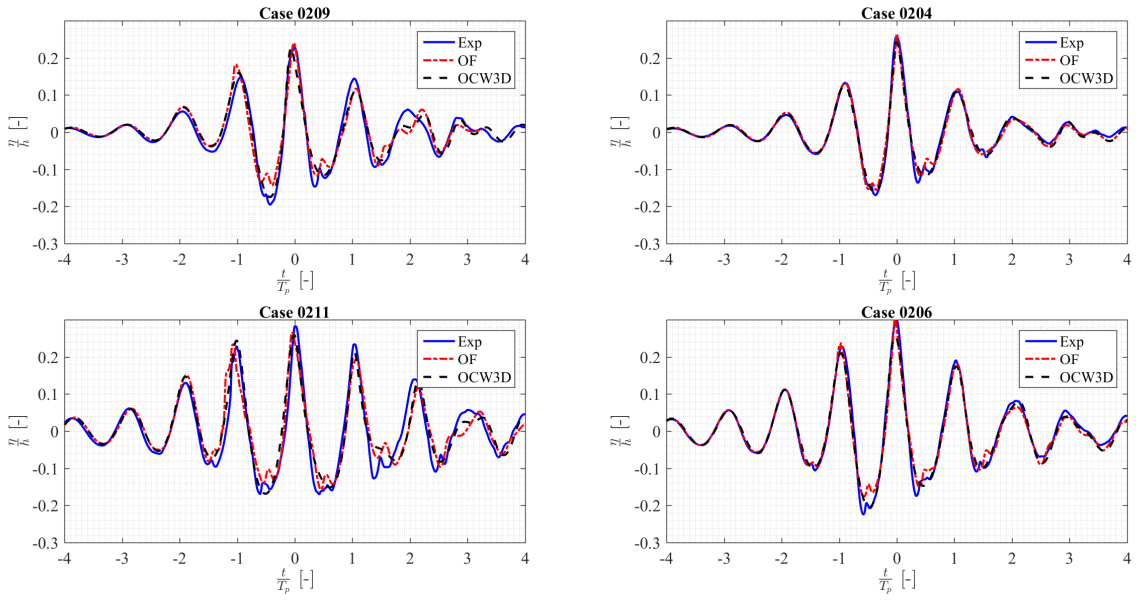

Figure 3: Non-dimensional free surface elevation time series at 7.1 m from the wave paddles.

3.2. In-line forces

Figure 4 shows the non-dimensional in-line force time series of the investigated cases. Similarly to the previous figure, the plots on the left hand side are for the 2D wave groups while the plots on the right hand side are for the 3D wave groups.

The measured in-line force time series show the same general behavior as the surface elevation plots presented in figure 3. It should be mentioned that unlike surface elevations that were measured and computed at 7.1 m from the wave paddles, the forces are measured and computed at the monopile location, 7.3 m from the wave paddles. Even though the surface elevations are measured 0.2 m up stream the monopile the in-line force time series maximize almost at the surface elevation focus time, $\frac{t}{Tp} = 0$. This is expected as the flow is inertia dominated. The Keulegan-Carpenter (KC) number is smaller than 6 in all cases [3]. For inertia dominated flows the force is in phase with $\dot{u}$ so 90 deg to u and η. Hence, the force peak can be expected to occur earlier than the arrival of the wave crest. For OceanWave3D, the in-line force was computed

with the Morison force model [3] with input of the undisturbed wave kinematics at x=7.3 m. The drag and inertia coefficient were 0.5 and 1.98 respectively, selected from experiment tables, Sumer and Fredsøe [3]. The OpenFOAM forces were obtained by direct pressure integration over the cylinder area.

Additionally to the main force peak, the force peak of the largest waves is seen to be followed by an additional peak, occuring in the trough of the force signal. These loads can be explained by the secondary load cycle [13, 18].

In addition, by comparison of the in-line force time series in figure 4 and the free surface elevation time series in figure 3 it is interesting to see that even though the waves are temporally symmetric, the forces time series are leaning backward. This can be explained by the effect of the inertia terms in the in-line forces, which is a well known feature of nonlinear wave loads.

Looking at figure 4 generally a good agreement between the measurements and forces computed in OceanWave3D can be seen. There are only seldom inconsistencies between the measurements and the numerical results. These inconsistencies are seen mostly at the troughs of the in-line force time series. However, a general inconsistency between the OceanWave3D results and the preceding wave crests can be seen in all cases except case 211. At this point the OceanWave3D result is always above the experiment results. This can be seen in the peak before the preceding peak of case 211 too ($\frac{t}{T_p} = -2$).

The most significant difference between the experiments and the OceanWave3D results is observed in the preceding trough of the focus wave in case 211 and the crest before that. Investigating the videos from the experiments it was observed that the wave breaks at this time and hence fills in the coming trough. This, obviously, cannot happen in the potential flow solver.

Comparing the measurements and the OpenFOAM results we can see that the CFD simulations of all cases are mostly consistent with the measurements. The only two inconsistencies are observed in the main focused wave in cases 209 and 204. In these cases the crests of the in-line forces of the focus waves are under predicted in CFD simulations.

For the steeper cases 206 and 211 the waves are breaking at impact time in the former case and is highly non-linear in the latter case. The peak loads, however, are predicted with good accuracy by the Navier-Stokes solver.

The additional peaks in the troughs of the in-line force time series, observed in the measurements, are also reproduced in the OpenFOAM simulation as seen in figure 4. It can also be seen that the backward inclination of the in-line forces are reproduced in the OceanWave3D and OpenFOAM simulation results.

It is worth mentioning that the preceding wave in case 211 shows the same behavior in the CFD results as in the experiments. A small crest on top of the crest can be seen which in the CFD solution, where the impacting wave is broken and have broken up to a series of smaller surface rollers on top of the main wave. However, the crest of the in-line force is under predicted in the OpenFOAM simulation. Another major inconsistency between the OpenFOAM results and the experiments is in the case of 206 in which the preceding and the following troughs of the focus wave are predicted to produce larger in-line forces.

To investigate these inconsistencies, the pressure distribution and time series are compared between the OpenFOAM results and the experiments.

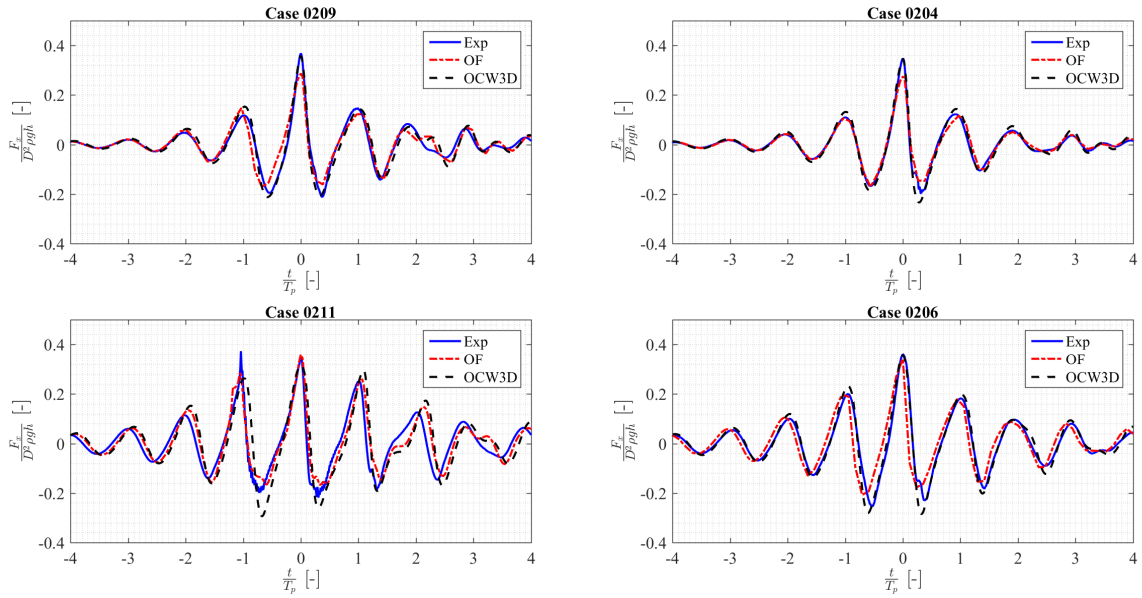

Figure 4: Non-dimensional in-line force time series at the location of the cylinder (7.3 m from the wave paddles).

4. Wave-induced pressure distribution at the cylinder

In figures 5 to 6 (left hand side) the contour plots of the wave induced pressure on the half cylinder is shown for the cases 211 and 206 for the time instant of maximum in-line force. The wave-induced pressure is here defined as

$$p_{\text{wave induced}} = \begin{cases} p_{\text{physical}} + \rho_{\text{water}} g z & z < 0 \\ p_{\text{physical}} & z > 0 \end{cases} \tag{2}$$

and is thus the physical pressure minus the pressure that would be present in case of still water. In the same plots the locations of the pressure sensors mounted on the cylinder in the experiments are marked with black circles. It should be noticed that in this plot the horizontal axis is the azimuthal position in relation to the cylinder. The cylinder faced the wave paddle at $\theta = 180\,\text{deg}$.

On the right hand side the wave induced pressure time series measured and computed from the OpenFOAM results are presented in five plots.

For the 2D wave (case 211) of figure 5, the pressure time series at the location of sensors below SWL show a similar behavior as the surface elevation time series. The time series related to the sensors above SWL, however, are sometimes hit by water (when the surface elevation is high enough) and sometimes they output constant zero pressure. It can be seen in these plots that the higher the location of the sensor is, the fewer waves in the wave group can reach to that height. Hence fewer peaks in the wave induced pressure time series is visible. Further, the magnitude of the peak pressure at the time of maximum in-line force ($t/T_p \approx 0$) decreases with height for the sensors above SWL.

For the two bottom sensors, the measured and computed pressure histories have the same general shape and magnitude, although with some over-prediction of the pressures in the troughs before and after the main focused wave.

For the next 2 sensors (located 0.08 m and 0.12 m above the SWL) there are only marginal inconsistencies between the measurements and computational results. The largest inconsistency can be seen at the location of the highest sensor, 0.16 m over SWL. In this case the time history

and peak pressure for the main focused wave is reproduced correctly in the CFD solution, while pressure of the the preceding and the following waves are under-estimated. This behavior, however, is consistent with the in-line force of the preceding wave shown in figure 4 which is at a broken stage at the time of impact.

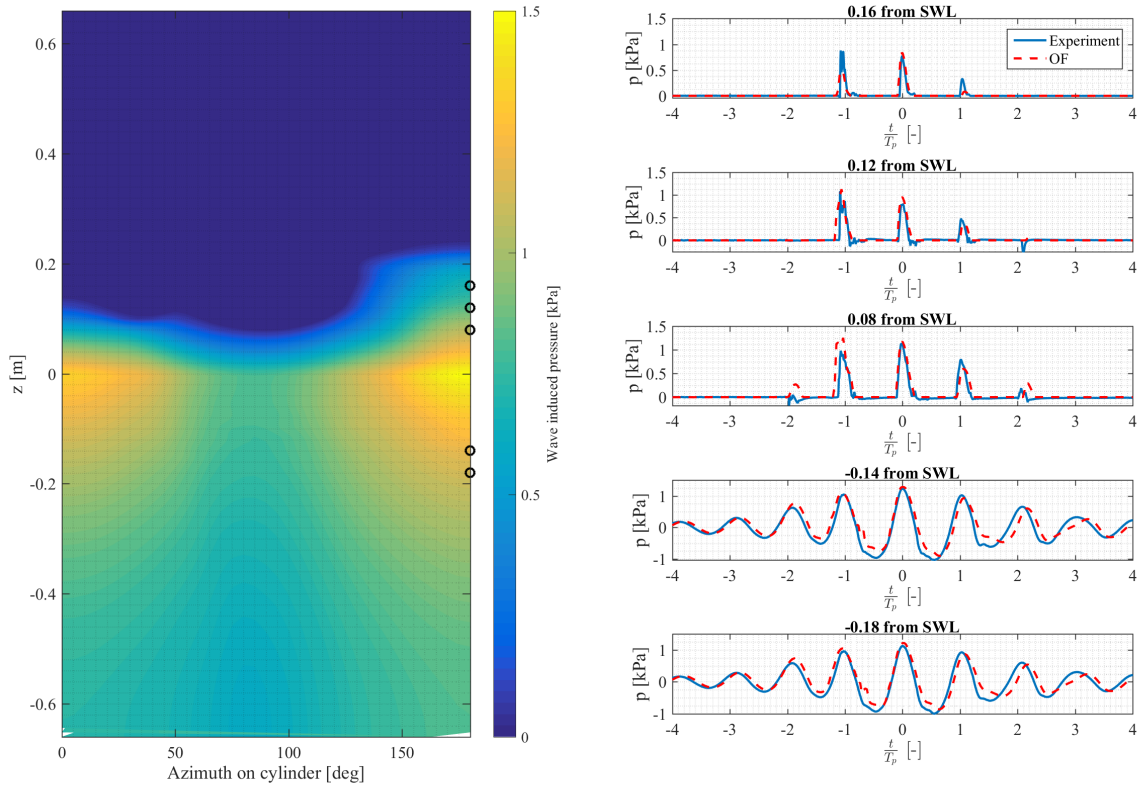

Figure 5: Dynamic pressure distribution contour plot (left hand side) and pressure time series measured and computed in the OpenFOAM at five different heights (right hand side). Case 211.

A similar comparison of experimental and numerical pressures for the 3D wave of case 206 is provided in figure 6. Similarly to the 2D case, the wave induced pressure in the troughs before and after the main focused wave are over-predicted in the numerical solution. This can explain the over prediction of in-line force in figure 4 case 206 in the preceding and the following wave troughs of the focus wave. Another significant difference between the OpenFOAM computed pressure and the measurements can be seen in the crest of the preceding waves at the location of the three sensors above the SWL. Both the experimental and numerical pressure signals contain multiple peaks following each other at a rapid time scale within the same wave event. While this indicates that the impacting wave is breaking, the breaking behaviour is seen to be differently distributed in height, since the experimental breaking is visible at the sensor at $z = 0.12$ m, while the numerical solution shows signs of breaking at the lower sensor at $z = 0.08$ m.

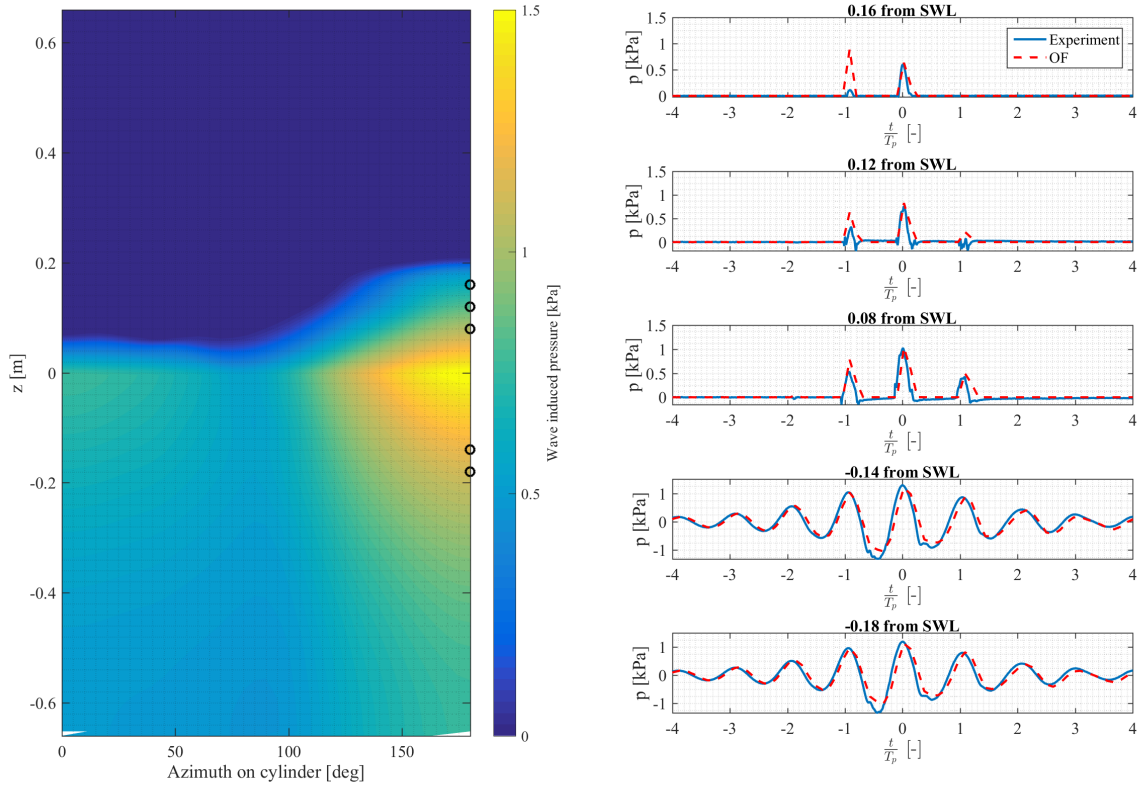

Figure 6: Dynamic pressure distribution contour plot (left hand side) and pressure time series measured and computed in the OpenFOAM at five different heights (right hand side). Case 206.

In figure 7 two snapshots of the impact of the focus waves for cases 211 and 206 are shown. In both snapshots the direction of the transmission of the waves is from right to left. On the left hand side, case 211, the build up of a water column behind the cylinder can be seen at the time of the impact. Subsequent back wash of the water around the cylinder is known to create the secondary load cycles. In the present case, the water column is created earlier than case 206. This can probably explain the high pressure region on the back side of the cylinder at the impact time shown in the contour plot in figure 5.

In the 3D case 206, the right hand side snapshot in figure 7, the wave is breaking at the impact time. At this time the backside stagnation pressure has not yet built up. Hence the pressure field is dominated by the front side as shown in the contour plot in figure 6.

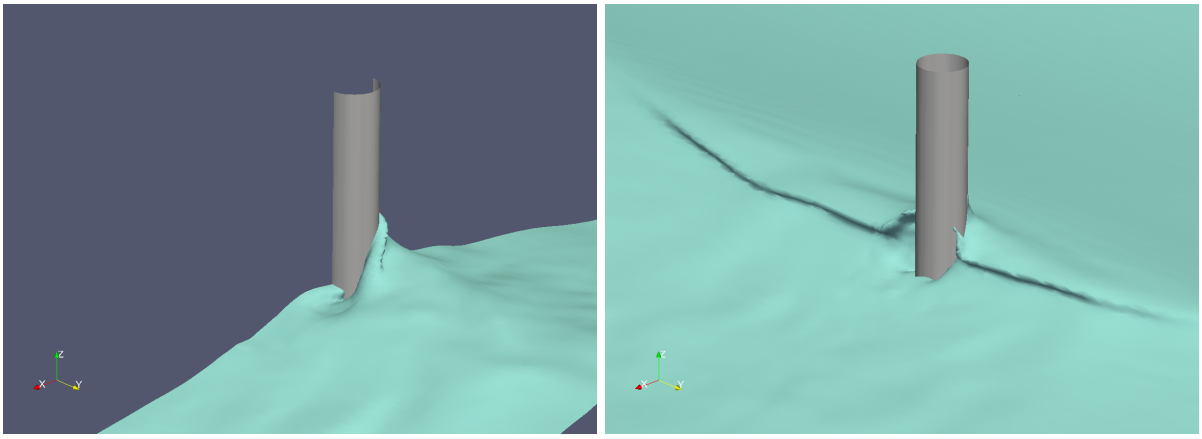

Figure 7: Snapshots of the free surface at the time of impact of the focus wave for cases 211 (left) and 206 (right).

5. Conclusion

In the present paper, wave impacts of steep and breaking focused wave groups have been investigated. Two numerical models have been used to reproduce four cases of focused wave groups; a potential flow solver (OceanWave3D) and a Navier-Stokes solver (OpenFOAM, using the toolbox Waves2FOAM). The waves were highly nonlinear and breaking. Two of the cases were 2D wave groups and two of them 3D wave groups. Both solvers provided a good reproduction of the free surface elevation for all four tests with only minor errors. Also for the in-line forces, a good match was found. Here, the OceanWave3D results, obtained by application of the Morison equation, followed the experimental force history closely, although no representation of wave-structure interaction can be achieved. The coupled solver, showed a slight under-prediction of the peak forces for the 2D and 3D groups of smallest amplitude, while the peaks for the main waves of the two large groups were well captured. The coupled solver further allowed a detailed reproduction of the wave-structure interaction which for the steep 2D case included the secondary load cycle of in-line force.

Point pressure measurements were also reproduced by the CFD solver and generally showed a good agreement with the tests, even above SWL. The spatial pressure fields for the largest 2D and 3D wave groups at the time of maximum force were discussed. The steep but non-breaking 2D impact created a strong run-up at the cylinder front, and a pronounced simultaneous pressure at the back side by stagnation of water. The 3D impact was breaking with similar strong pressures at the front side, but with no counter-acting stagnation pressure at the back. More investigation, for pressure distributions at the cylinder wall is therefore intended for a larger range of wave conditions.

The coupled solver allows computation of wave impacts for realistic open ocean wave fields. Further development of the model includes a refined breaking filter within the OceanWave3D solver which might improve the accuracy for cases where the waves that break inside the coupling zone between the two models. These investigations, together with further analysis of bending moments and pressure fields will contribute to improved accuracy in the numerical prediction of ULS wave loads for offshore wind turbines.

6. Acknowledgement

The present research was partly funded by the DeRisk project of Innovation Fund Denmark, grant number 4106-00038B. Further funding was provided by Statoil, DHI and DTU. All funding is gratefully acknowledged.

References

[1] Dean R G 1965 *Journal of Geophysical Research* **70** 4561 – 4572
[2] Christensen E D, Bredmose H and Hansen E A 2005 Extreme wave forces and wave run-up on offshore wind-turbine foundations *Copenhagen Offshore Wind Conference* 1995 pp 1–10
[3] Sumer B and Fredsøe J 1997 *Hydrodynamics Around Cylindrical Structures* Advanced series on ocean engineering (World Scientific)
[4] Bredmose H, Skourup J, Hansen E, Christensen E D, Pedersen L and Mitzlaff A 2006 Numerical reproduction of extreme wave loads on a gravity wind turbine foundation *OMAE2006*
[5] Bredmose H and Jacobsen N G 2010 Breaking wave impacts on offshore wind turbine foundations: focused wave groups and CFD *OMAE2010*
[6] Bredmose H and Jacobsen N G 2011 Vertical wave impacts on offshore wind turbine inspection platforms *OMAE2011*
[7] Hildebrandt A and Schlurmann T 2012 Breaking Wave Kinematics, Local Pressures, and Forces on a Tripod Structure *Coastal Engineering Conference* vol 1
[8] Bredmose H, Dixen M and Ghadirian A 2016 DeRisk - Accurate Prediction of ULS Wave Loads. Outlook and First Results *EERA DeepWind'2016*
[9] Engsig-Karup A, Bingham H and Lindberg O 2009 *Journal of Computational Physics* **228** 2100 – 2118
[10] Jacobsen N, Fuhrman D and FredsœJ 2012 *International Journal for Numerical Methods in Fluids* **70** 1073–1088
[11] Paulsen B T, Bredmose H and Bingham H 2014 An efficient domain decomposition strategy for wave loads on surface piercing circular cylinders *Coastal Engineering Conference* vol 86 pp 57 – 76
[12] Paulsen B T 2013 *Efficient computations of wave loads on off shore structures* Ph.D. thesis
[13] Paulsen B T, Bredmose H, Bingham H and Jacobsen N 2014 *Journal of Fluid Mechanics* **755** 1–34
[14] Zang J, Taylor P H and Tello M 2010 Steep Wave and Breaking Wave Impact on Offshore Wind Turbine Foundations - Ringing Re-visited *International Workshop on water waves and floating bodies IWWWFB2010*
[15] Hirt C and Nichols B 1981 *Journal of Computational Physics* **39** 201–225
[16] Clauss G F, Schmittner C E and Hennig J 2006 Systematically varied rogue wave sequences for the experimental investigation of extreme structures *OMAE2006*
[17] Goda Y 2010 *Coastal Engineering Journal* **52** 71–106
[18] Grue J and Huseby M 2002 *Applied Ocean Research* **24** 203 – 214